Chemical effects of carbon dioxide sequestration in the Upper Morrow Sandstone in the Farnsworth, Texas, hydrocarbon unit

Bulbul Ahmmed, Martin S. Appold, Tianguang Fan, Brian J. O. L. McPherson, Reid B. Grigg, and Mark D. White

ABSTRACT

Numerical geochemical modeling was used to study the effects on pore-water composition and mineralogy from carbon dioxide (CO_2) injection into the Pennsylvanian Morrow B Sandstone in the Farnsworth Unit in northern Texas to evaluate its potential for long-term CO_2 sequestration. Speciation modeling showed the present Morrow B formation water to be supersaturated with respect to an assemblage of zeolite, clay, carbonate, mica, and aluminum hydroxide minerals and quartz. The principal accessory minerals in the Morrow B, feldspars and chlorite, were predicted to dissolve. A reaction-path model in which CO_2 was progressively added up to its solubility limit into the Morrow B formation water showed a decrease in pH from its initial value of 7 to approximately 4.1 to 4.2, accompanied by the precipitation of small amounts of quartz, diaspore, and witherite. As the resultant CO_2-charged fluid reacted with more of the Morrow B mineral matrix, the model predicted a rise in pH, reaching a maximum of 5.1 to 5.2 at a water–rock ratio of 10:1. At a higher water–rock ratio of 100:1, the pH rose to only 4.6 to 4.7. Diaspore, quartz, and nontronite precipitated consistently regardless of the water–rock ratio, but the carbonate minerals siderite, witherite, dolomite, and calcite precipitated at higher pH values only. As a result, CO_2 sequestration by mineral trapping was predicted to be important only at low water–rock ratios, accounting for a maximum of 2% of the added CO_2 at the lowest water–rock ratio investigated of 10:1, which corresponds to a small porosity increase of approximately 0.14% to 0.15%.

Manuscript received May 26, 2015; provisional acceptance September 3, 2015; revised manuscript received March 21, 2016; final acceptance May 13, 2016.

DOI:10.1306/eg.09031515006

AUTHORS

BULBUL AHMMED ~ *Department of Geological Sciences, 101 Geological Sciences Building, University of Missouri, Columbia, Missouri 65211; bulbul_ahmmed@baylor.edu*

Bulbul Ahmmed received his B.S. in geology from the University of Dhaka, Bangladesh, in 2011 and his M.S. in geological sciences from the University of Missouri–Columbia in 2015. He is currently a Ph.D. student in geology at Baylor University, where he is studying hydraulic fracture networks in low-permeability rocks using the electrical resistivity method.

MARTIN S. APPOLD ~ *Department of Geological Sciences, 101 Geological Sciences Building, University of Missouri, Columbia, Missouri 65211; appoldm@missouri.edu*

Martin Appold is an associate professor in the Department of Geological Sciences at the University of Missouri–Columbia. He received a B.A. in geology from Washington University, an M.S. in economic geology from the University of Michigan, and a Ph.D. in hydrogeology from Johns Hopkins University. His main research interests are the physical and chemical behavior of subsurface fluids.

TIANGUANG FAN ~ *Petroleum Recovery Research Center, New Mexico Institute of Mining and Technology, 801 Leroy Place, Socorro, New Mexico 87801; tfan@nmt.edu*

Tianguang Fan is a research chemist in the Petroleum Recovery Research Center at the New Mexico Institute of Mining and Technology. He earned a B.S. in engineering from the East China University of Science and Technology and an M.S. in chemistry from the New Mexico Institute of Mining and Technology.

BRIAN J. O. L. MCPHERSON ~ *Department of Civil and Environmental Engineering, University of Utah, 110 Central Campus Drive, Suite 2000, Salt Lake City, Utah 84112; bmcpherson@egi.utah.edu*

Brian McPherson is a professor in the Department of Civil and Environmental Engineering at the University of Utah and coprincipal investigator of the Southwest Regional Partnership on Carbon Sequestration. He received a B.S. in geophysics

from the University of Oklahoma and an M.S. and a Ph.D. in geophysics from the University of Utah. His technical focus areas include simulation of multiphase flow, rock deformation, and reactive transport.

REID B. GRIGG ~ *Petroleum Recovery Research Center, New Mexico Institute of Mining and Technology, 801 Leroy Place, Socorro, New Mexico 87801; reid@prrc.nmt.edu*

Reid Grigg is a retired senior engineer in the Petroleum Recovery Research Center at the New Mexico Institute of Mining and Technology and former coprincipal investigator of the Southwest Regional Partnership on Carbon Sequestration. He received a Ph.D. in physical chemistry from Brigham Young University. His principal research interests are petroleum reservoir engineering and carbon sequestration.

MARK D. WHITE ~ *Pacific Northwest National Laboratory, 902 Battelle Boulevard, P.O. Box 999, MSIN K9-33, Richland, Washington 99352; mark.white@pnnl.gov*

Mark White is a staff engineer in the Hydrology Technical Group at Pacific Northwest National Laboratory and the senior author of the STOMP simulation software. He received a B.S. in biophysics from Pennsylvania State University and an M.S. and a Ph.D. in mechanical engineering from Colorado State University. His principal research interests are the development and application of scientific computer codes for modeling multifluid, coupled processes in geologic media.

ACKNOWLEDGMENTS

Funding for this work was provided by US Department of Energy Contract DE-FC26-05NT42591. We would like to thank Chaparral Energy, Inc., for permission to publish this work.

INTRODUCTION

Injection of carbon dioxide (CO_2) into mature hydrocarbon reservoirs is a long-standing method for enhanced oil recovery (EOR) and is becoming an increasingly attractive strategy for CO_2 sequestration (Harrison and Falcone, 2014; Verma, 2015). The Morrow B Sandstone member of the Pennsylvanian Upper Morrow Sandstone in the Farnsworth Unit (FWU), a hydrocarbon field in northern Texas, United States, has been selected for a demonstration of commercial-scale CO_2 EOR by the US Department of Energy's Southwest Partnership on CO_2 Sequestration. Hydrocarbon production from FWU began in 1956 and yielded 39,600,000 bbl (~6.3 million m^3) of oil and approximately 29,000,000 MCF (~8.2×10^8 m^3) of natural gas as of February 28, 2015. Most of this production—36,300,000 bbl (5.7 million m^3) of oil—occurred as of November 30, 1986 (Munson, 1989). Since then, 1,800,000 bbl (289,000 m^3) of oil were produced until CO_2 flooding began on November 30, 2010. The CO_2 flooding through February 28, 2015, produced another 1,500,000 bbl (~231,000 m^3) of oil. Since 1986, only approximately 200,000 MCF (5.66×10^6 m^3) of gas have been produced. Chaparral Energy has operated the FWU since December 2009, and the Southwest Partnership began its collaborative demonstration project at FWU in April 2013.

In the subsurface, CO_2 may be sequestered by several trapping mechanisms, including structural, capillary, solubility, and mineral trapping (Intergovernmental Panel on Climate Change, 2005). Mineral trapping is a particularly favorable form of CO_2 sequestration because of its simple outcome product: stable mineral solids (Gunter et al., 1997; Oelkers et al., 2008). However, mineral precipitation and/or dissolution may also impact the porosity and permeability of the reservoir, even during very short time scales, and thus affect injectivity, productivity, and fluid dynamics. Thus, predicting how CO_2 injection will change the Morrow B pore-water composition, mineralogy, porosity, and permeability is important for evaluating the feasibility of large-scale CO_2 sequestration in the Morrow B in the FWU.

The FWU lies within the well-studied Anadarko basin. Despite the extensive existing geological literature coverage of the broader basin, little direct work on the FWU has been published. Previous works include publications by Parker (1956), Munson (1989), McKay and Noah (1996), and Ampomah et al. (2015) and unpublished masters' theses by Munson (1988) and Gallagher (2014) about the deposition, mineralogy, diagenesis, reservoir properties, and production history of the Morrow B Sandstone.

This paper is FWU specific but is broadly applicable to the Morrow Sandstone in the Anadarko basin. Our objective is to present initial results and interpretations of equilibrium geochemical speciation and reaction-path modeling for CO_2 injected into the Morrow B Sandstone within the FWU. More specifically, we seek to

answer three questions. (1) How will the composition of the Morrow B pore water and rock matrix change as a result of CO_2 injection? (2) How much CO_2 could be expected to be sequestered by mineral trapping? (3) How much might the hydraulic properties of the Morrow B Sandstone be altered by CO_2 injection? Our models did not consider the presence of oil, some of which could dissolve into the formation water and slightly reduce the solubility of CO_2.

GEOLOGIC BACKGROUND

The FWU is located in the western part of the Anadarko basin (Figure 1), historically one of the most important hydrocarbon-producing regions in the United States. The Morrow Sandstone was deposited during the third main stage of Anadarko basin evolution, in which Pennsylvanian orogeny led to uplift of the Wichita–Amarillo block on the basin's southern margin, accompanied by downwarping within the basin, allowing the accumulation of approximately 5500 m (18,000 ft) of mostly marine sediments (Johnson, 1989). Epeirogenic sediment deposition has characterized the subsequent fourth stage of basin evolution, which is preserved mainly as approximately 2000 m (6600 ft) of Permian red beds and evaporites. The first two stages of basin evolution consisted of Early to Middle Cambrian emplacement of igneous rocks upon 1300 to 1600 Ma basement rock, followed by Late Cambrian through Mississippian deposition of approximately 4500 m (15,000 ft) of sediments consisting of mainly carbonates and lesser amounts of fine- to medium-grained clastics.

In the FWU, the Morrow Sandstone has an average thickness of approximately 275 m (900 ft) and has been subdivided into a lower, middle, and upper section (Munson, 1989; Figure 2). The Lower Morrow consists of a transgressive series of shallow marine claystones, sandstones, and limestones that unconformably overlie Mississippian Chester Group sedimentary rocks. The Middle Morrow consists of mainly carbonate and shale with minor sandstone. The Upper Morrow consists of approximately 115–150 m (380–490 ft) of mainly shales that contain lenticular, discontinuous, coarse-grained sandstones, reflecting a fluvial deltaic environment that prograded toward the southeast (Swanson, 1979).

Most of the hydrocarbon production from FWU has come from the Morrow B Sandstone, the sole formation undergoing CO_2 injection for EOR. The Morrow B lies at a depth of approximately 2400 m (7900 ft), at a temperature of 75°C (167°F), and with an initial reservoir pressure reported at 15.2 MPa (2200 psi), conditions under which CO_2 should exist in a supercritical state for increased storage efficiency (Munson, 1989; Bergman and Winter, 1995; Bergman et al., 1997; Bachu, 2002). Porosity in the Morrow B reportedly ranges from approximately 10% to 18%, with an average of 14.5%, and permeability ranges from approximately

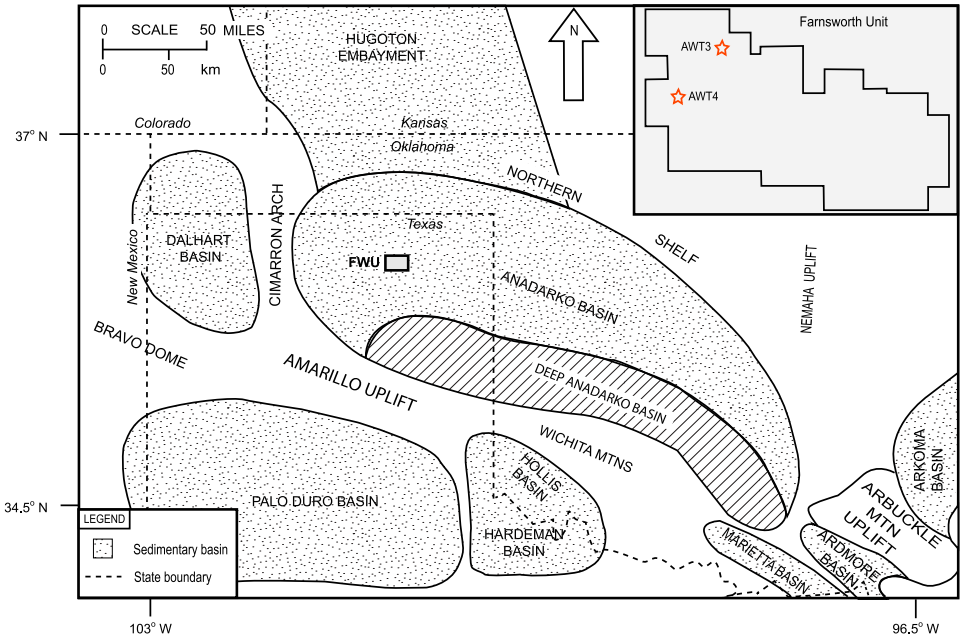

Figure 1. Geologic context and location of the Farnsworth Unit (FWU; modified after Johnson, 1989). Inset in the upper-right corner shows the outline of the FWU and the locations of the wells sampled by well batteries AWT3 and AWT4. MTN = mountain.

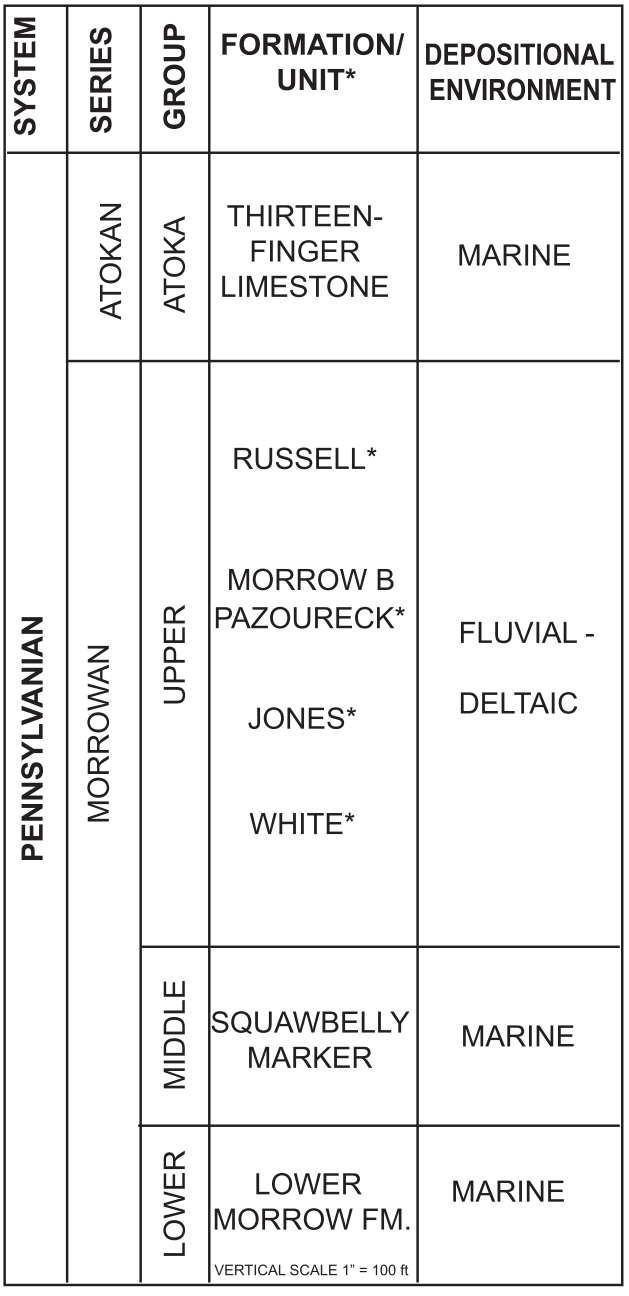

Figure 2. Stratigraphic chart showing divisions of the Upper Morrowan and Lower Atokan strata in the Farnsworth Unit. Wireline log is from well 32-2. Modified from Munson (1989) and Puckette et al. (2008) by Gallagher (2014). FM. = formation.

1 to 250 md, with an average of 48 md (Munson, 1989; Ampomah et al., 2015). Both porosity and permeability tend to be higher in the western half than in the eastern half of the FWU. The Morrow B Sandstone averages 9 m (30 ft) in thickness, with a maximum of approximately 16 m (52 ft), and consists of mainly quartz, with minor plagioclase feldspar and clay minerals and traces of calcite, siderite, ankerite, and dolomite. The clay minerals consist of mainly kaolinite and chlorite, with minor illite and traces of smectite. The initial water saturation in the Morrow B at the time of the discovery of the FWU was 31.4% (Ampomah et al., 2015), and the Morrow B remains water wet, allowing ample opportunity for water–rock chemical reactions.

Conformably overlying the Upper Morrow is the Thirteen Finger Limestone, an aquitard and the lowest member of the Pennsylvanian Atoka Series. The base of the Thirteen Finger consists of a thin coal bed overlain by finely crystalline dolomitic limestones and shales. The thickness of the Thirteen Finger averages approximately 40 m (130 ft) in the FWU, increasingly slightly from west to east (Higley, 2011).

METHODOLOGY

All geochemical speciation and reaction-path modeling calculations were based on Morrow B Sandstone pore-water samples collected from well batteries AWT3 and AWT4 on September 24, 2012; January 15, 2013; and April 11, 2013. Well batteries AWT3 and AWT4 have the capability to draw water from multiple wells across the western half of the FWU, but in the present study they drew water from only wells 11-2 and 9-7, respectively. Water samples were collected in 1-L, wide-mouth, high-density polyethylene bottles. To ensure that clean and representative pore-water samples were collected, water lines were thoroughly flushed before sampling. After collection, water samples were immediately placed in a simple cooler (Igloo brand), and upon returning to the laboratory they were filtered through a 0.22-μm syringe filter to remove oil and dirt. Filtered water samples were typically analyzed for chemical composition within 1–2 wk of collection in the field.

The pH and oxidation-reduction potential (ORP) of water samples were measured in the field using a Thermo Fisher Dual Star Benchtop pH/ISE meter, an Orion 8102BNUWP glass combination pH electrode, and an Orion 9179BN Triode Low Maintenance ORP electrode. Water conductivity was measured using an Orion Model 162A conductivity meter and an Orion 01801A conductivity cell. Water alkalinity was measured with electrometric titration following the American Society for Testing and Materials (ASTM) D1067-02 method. The concentrations of major cations Li^+, Na^+, K^+, Mg^{2+}, and Ca^{2+} and major anions F^-, Cl^-, Br^-, NO_3^{2-}, and SO_4^{2-} were determined by ion chromatography

Table 1. Composition of Pore Water Sampled from Well Batteries AWT3 and AWT4 and Employed in the Modeling

Basis Species	AWT3 (mg/kg in fluid)	AWT4 (mg/kg in fluid)
Al^{+++}	1.05	0.00791
$B(OH)_3$ (aq)	21.5	27.8
Ba^{++}	0.592	1.37
Br^-	17.8	20.3
Ca^{++}	38.5	32.9
Cl^-	1.47E+03	1.84E+03
F^-	0.654	0.911
Fe^{++}	7.29E-05	2.10E-08
HCO_3^-	5.79E+04	795
K^+	7.87	7.11
Li^+	0.283	0.461
Mg^{++}	6.27	12.3
Na^+	1.08E+03	1.41E+03
SO_4^{2-}	21.4	12.9
SeO_3^{2-}	0.0687	0.0827
SiO_2 (aq)	24.5	42.1
Sr^{++}	2.68	1.85
Zn^{++}	1.51E-05	0.108
pH	7	7
ORP (mV)	140	140

Abbreviations: Al = aluminum; aq = aqueous; Ba = barium; Br = bromine; $B(OH)_3$ = boric acid; Ca = calcium; Cl = chlorine; Eh = reduction–oxidation potential; F = fluorine; Fe = iron; HCO_3^- = bicarbonate; K = potassium; Li = lithium; Mg = magnesium; Na = sodium; SiO_2 = silicon dioxide; SeO_3^{2-} = selenite ion; SO_4^{2-} = sulfate; Sr = strontium; Zn = zinc.

using a Dionex DX-120 equipped with an IonPac CS-12A column for cation analysis and an IonPac AS9-HC column for anion analysis, following ASTM methods D6910-03 and D4327. Water samples were sent to the New Mexico Bureau of Geology and Mineral Resources to determine trace metal concentrations using inductively coupled plasma mass spectrometry following US Environmental Protection Agency Method 200.8 (Creed et al., 1994).

The time-averaged compositions of pore water from each well used in the modeling are listed in Table 1. Aluminum (Al) and iron (Fe) concentrations were obtained by assuming saturation with respect to illite and hematite, respectively, because neither element was detected in the compositional analyses. The relative mineral abundances and porosity of the Morrow B, for purposes of reaction-path modeling, were based on the analyses of Munson (1989) and Gallagher (2014) and are summarized in Table 2. The reservoir temperature of 75°C (167°F) was assumed for all calculations.

All of the chemical modeling calculations were conducted using Geochemist's Workbench® software and the thermo.com.v8.r6+ thermodynamic database for pressures and temperatures on the liquid–vapor saturation (boiling) curve for water. The resultant model fluid pressure of 0.039 MPa (5.6 psi) at 75°C (167°F) is significantly lower than the actual initial reservoir pressure of 15.2 MPa (2200 psi). Reactions that are likely to be most sensitive to this pressure discrepancy involve gas species, so, for this study, the equilibrium constant for the CO_2 gas formation reaction in the thermo.com.v8.r6+ database was replaced with the value corresponding to 15.2 MPa (2200 psi) and 75°C (167°F), calculated using the SUPCRT92b software (Johnson et al., 1992). The difference in log K values at water saturation versus reservoir pressure at 75°C (167°F) was small. In this simulation, the log K value of –8.769 corresponding to 15.2 MPa (2200 psi) of pressure was used instead of the original log K value of –8.776 corresponding to 0.039 MPa (5.6 psi) of pressure.

Speciation calculations were first carried out to learn what minerals should be expected to precipitate or dissolve given the current composition of the Morrow B pore fluid prior to the scheduled CO_2 injection. Reaction-path models were then simulated to explore the possible effects of CO_2 on the composition of the Morrow B pore fluid and to determine how the CO_2-charged pore fluid would react with the host rock. Reaction-path modeling included two stages. In stage 1, CO_2 was gradually added to Morrow B Sandstone pore water up to its solubility limit of 46 g/kg water at 75°C (167°F), 15 MPa (2175 psi), and 1 M sodium chloride salinity (Duan and Sun, 2003). The resultant CO_2-saturated pore water

Table 2. Mineral Composition of the Morrow B Sandstone Employed in the Modeling Based on the Average of Petrographic Characterizations by Munson (1989) and Gallagher (2014)

Minerals	Volume (%)
Quartz	84.26
Albite	9.0
Calcite	0.75
Ankerite	0.25
Siderite	0.25
Montmorillonite	0.1
Illite	0.88
Chlorite	1.79
Kaolinite	2.72

was then allowed to react with the Morrow B host-rock mineralogy (Table 2).

Two scenarios were considered for stage 2 of the reaction-path modeling—one in which the CO_2-saturated pore fluid was allowed to react with enough rock to create a 1% increase in porosity if all of that rock dissolved (i.e., a 100:1 volumetric water–rock ratio) and the other in which the CO_2-saturated pore fluid was allowed to react with enough rock to create a 10% increase in porosity if all of that rock dissolved (i.e., a 10:1 volumetric water–rock ratio). This led to masses of reactant rock of 27 and 270 g (0.060 and 0.60 lb), respectively, per kilogram of water, for a porosity of 14.5% and a bulk rock density of 2700 kg/m^3 (168.6 lb/ft^3). The actual change in porosity that resulted in the two model scenarios differed from 1% and 10%, because much of the dissolved rock reprecipitated, though not necessarily as the same minerals that were dissolved.

All of the reaction-path models were calculated assuming chemical equilibrium. These results therefore represent the maximum extent of chemical reaction possible while also showing the evolution of fluid chemistry and host-rock mineralogy en route to this maximum. Thus, although the results of the present study do not convey the time scale over which mineral sequestration would occur in the FWU, they place a limit on how much mineral sequestration can be expected and serve as a useful benchmark for planned future studies that will employ reaction kinetics and transient fluid flow and solute transport.

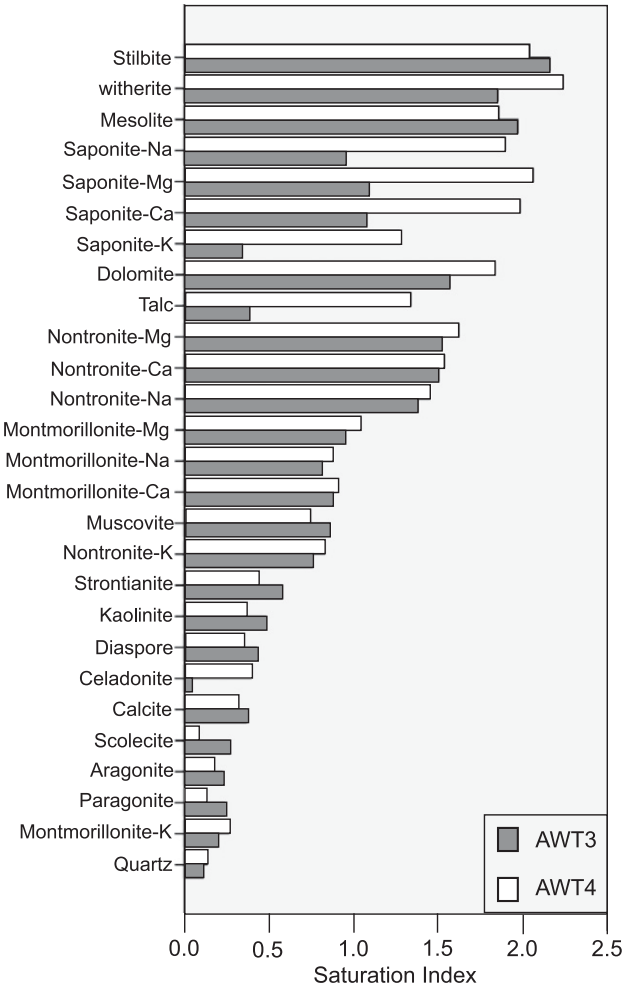

Figure 3. Minerals predicted to be supersaturated in Morrow B Sandstone formation water sampled from well batteries AWT3 and AWT4. Ca = calcium; K = potassium; Mg = magnesium; Na = sodium.

RESULTS

Speciation Modeling

Current Morrow B Sandstone groundwater is relatively dilute given its depth of approximately 2400 m (7900 ft), with a total dissolved solids (TDS) content of approximately 3600 mg/L that is dominated by sodium (Na), calcium (Ca), chlorine (Cl), and bicarbonate. The low salinity reflects the effects of water flooding, which was carried out intermittently until November 2010. Geochemical speciation modeling employed an ORP value of 140 mV and a pH of 7 for fluid compositions from both well batteries, AWT3 and AWT4, based on the averages of the water samples collected (Table 1). The results showed the Morrow B formation water to be supersaturated with respect to mainly zeolite minerals (stilbite, mesolite, scolecite), clay minerals (saponite, montmorillonite, nontronite, kaolinite, beidellite), carbonate minerals (witherite, dolomite, strontianite, calcite, aragonite), mica minerals (muscovite, paragonite, celadonite), and aluminum hydroxides (diaspore, boehmite; Figure 3). The predicted zeolite–smectite-rich mineral assemblage is typical of burial diagenetic environments (Hay, 1986), and these clay minerals were reported by Munson (1989) and Gallagher (2014) to be present in the Morrow B Sandstone. The clay minerals are likely to be alteration products of feldspars, because K-feldspar, albite, and anorthite were all predicted to be undersaturated in the Morrow B pore fluid (Figure 4). In contrast, quartz was predicted to be close to saturation,

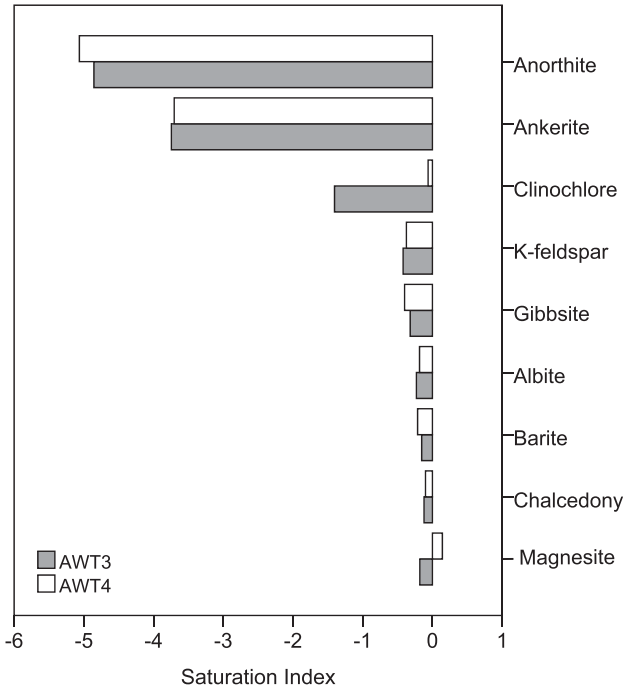

Figure 4. Minerals predicted to be undersaturated in Morrow B Sandstone formation water sampled from well batteries AWT3 and AWT4. K = potassium.

consistent with the quartz-rich nature of the Morrow B Sandstone.

Reaction-Path Modeling: Stage 1

In stage 1 of the reaction-path modeling, CO_2 was progressively added to 1 kg of Morrow B pore water up to the solubility limit of CO_2 of 46 g/kg (0.046 lb CO_2/lb water) under initial reservoir conditions (Duan and Sun, 2003). Calculations were carried out for initial fluid compositions corresponding to Morrow B pore water sampled from both well batteries, AWT3 and AWT4 (Table 1).

The progressive addition of CO_2 caused a corresponding decrease in pH from 7 to a minimum of 4.1 and 4.2 in the AWT3 and AWT4 model pore fluids, respectively, at CO_2 saturation (Figure 5). In the reaction-path models, the initial state of the system (at $\xi = 0$, where ξ is the reaction-progress variable) was reset by decreasing the pH to approximately 6.75 and reducing the carbonate alkalinity by approximately 13% to 16% for model fluids AWT3 and AWT4, respectively, so that no supersaturated minerals existed. In the resulting modified initial state, strontianite, quartz, dolomite, and witherite were at saturation for model fluid AWT4, and these minerals plus Ca-nontronite and mesolite were at saturation for model fluid AWT3.

Few further changes in mineralogy were predicted as more CO_2 was added to the pore fluids (Figure 6). The abundance of quartz remained constant at approximately 2×10^{-4} mol/kg water for both model fluids as CO_2 was added. With the exceptions of dolomite and witherite, all of the minerals that were produced in the initial state equilibration completely dissolved away with the first pH decrease and therefore do not appear among predicted mineral precipitates during stage 1 reaction-path modeling (Figure 6). For model fluid AWT4, dolomite persisted until the pH decreased to 6.13 at an ξ value of only 0.01. Diaspore was the only new mineral predicted to form as a result of CO_2 addition and precipitated early in the reaction path for both fluids. For model fluid AWT3, diaspore abundance remained relatively constant at approximately 5×10^{-5} mol/kg water, whereas, for AWT4, diaspore reached a maximum abundance of approximately 4×10^{-8} mol/kg water at $\xi = 0.1$, decreasing thereafter until its disappearance after $\xi = 0.65$. Witherite declined steadily in abundance over the reaction path for both model fluids from a maximum of approximately 10^{-5}, disappearing by $\xi = 0.1$ for model fluid AWT3 and by $\xi = 0.27$ for model fluid AWT4.

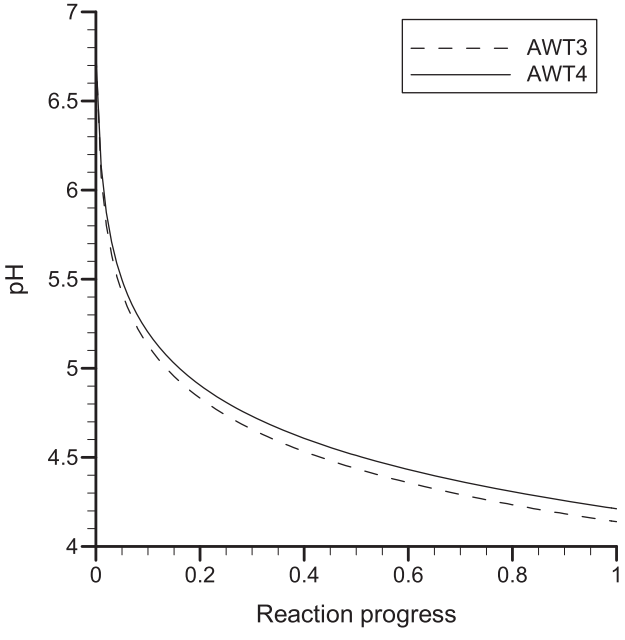

Figure 5. Predicted change in pH of Morrow B Sandstone formation water during stage 1 reaction-path modeling.

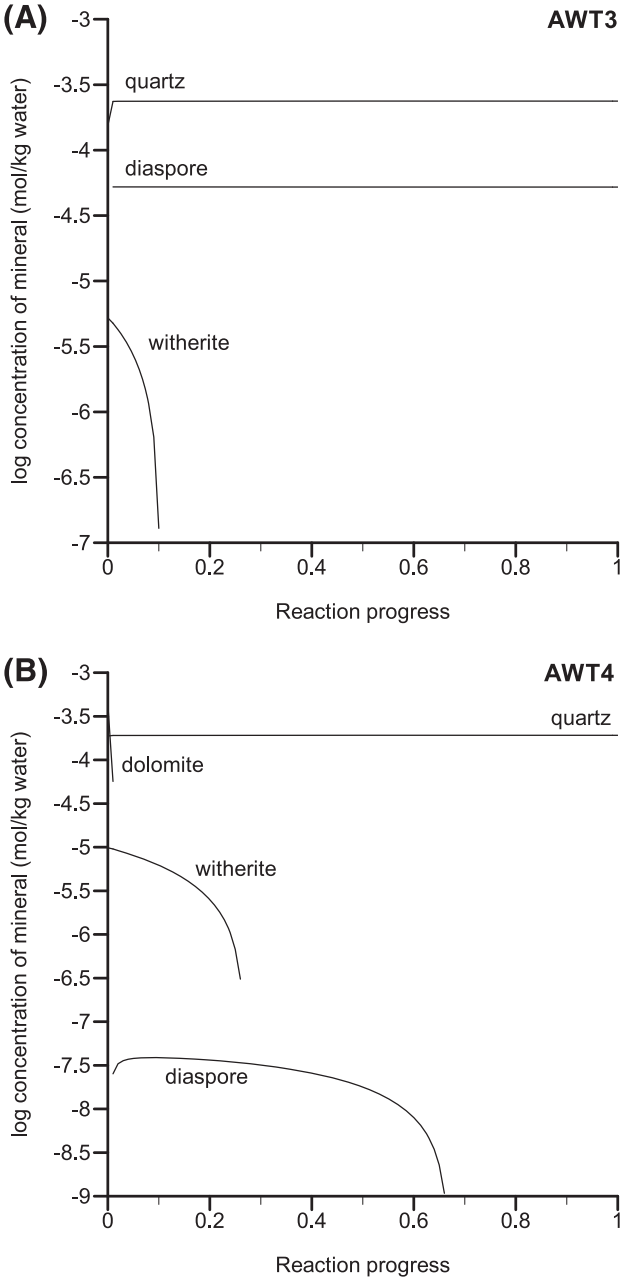

Figure 6. Predicted mineral precipitation during stage 1 reaction-path modeling for model fluid (A) AWT3 and (B) AWT4.

Reaction-Path Modeling: Stage 2

In stage 2 of reaction-path modeling, CO_2-charged fluid was allowed to react with Morrow B host rock in volumetric water–rock ratios of 100:1 and 10:1. The initial pH and CO_2 concentration were assigned directly from results of the stage 1 reaction-path model at CO_2 saturation. The initial pH value was 4.1 for the AWT3 fluid and 4.2 for the AWT4 fluid. The initial CO_2 concentration for both fluids was 1 mol/kg.

Figure 7 shows simulated pH as a function of reaction progress for model fluids AWT3 and AWT4 for volumetric water–rock ratios of 100:1 and 10:1. The results for the two model fluids are similar, but the pH

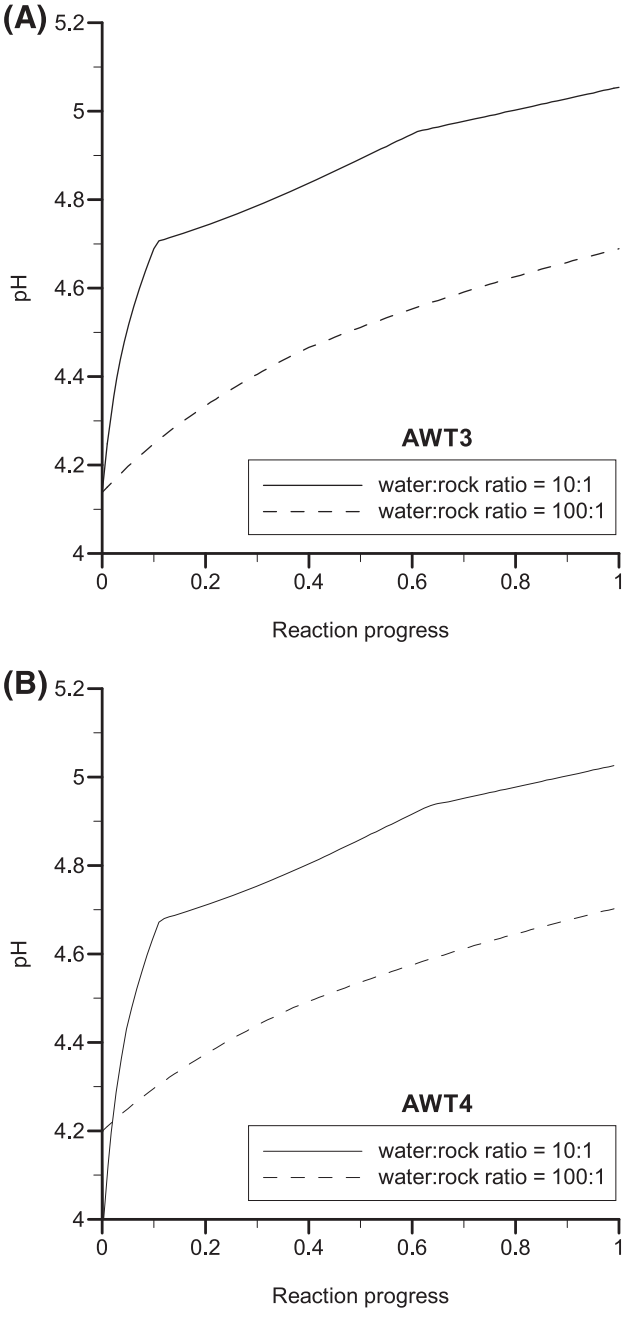

Figure 7. Predicted change in pH during stage 2 of the reaction-path modeling for model fluids (A) AWT3 and (B) AWT4 for final water–rock ratios of 100:1 and 10:1.

rose to a slightly higher level of 5.1 to 5.2 for the lower water–rock ratio case compared with approximately 4.7 for the higher water–rock ratio case. The increase in pH is caused by the consumption of minerals like calcite and albite, which react with H^+ to form bicarbonate and clay and aluminum hydroxide alteration minerals like nontronite and diaspore (Figure 8). Because more rock was available for reaction in the lower water–rock ratio scenario, the pH was buffered to a higher value.

The aluminum hydroxide mineral, diaspore, was predicted to be the principal alteration mineral formed in all of the reaction-path models, accounting for up to 0.22 mol/kg water by the end of the AWT3 reaction-path model for a 10:1 water–rock ratio (Figure 8B). In contrast, magnesium (Mg)-nontronite, which converted to Ca-nontronite as reaction with the host rock increased, was predicted to be orders of magnitude less abundant than diaspore. Siderite was also consistently predicted to form, precipitating in trace amounts up to approximately 10^{-3} mol/kg water for a 100:1 water–rock ratio and 10^{-2} mol/kg for a 10:1 water–rock ratio. Witherite was predicted to precipitate in both model fluids for both water–rock ratios, reaching a maximum concentration of approximately 10^{-5} mol/kg water. Moderate amounts of dolomite and calcite—up to approximately 0.045 mol/kg water—were predicted to precipitate in both model fluids at a water–rock ratio of 10:1, with calcite precipitation beginning significantly later than dolomite precipitation.

Several reactant minerals consistently reprecipitated as products. The most important of these is quartz, which remained saturated throughout all of the simulations. The final amount of quartz precipitated was slightly larger than the amount of reactant quartz, because some quartz formed through the dissolution of other reactant silicate minerals. After a period of dissolution, siderite reprecipitated after enough

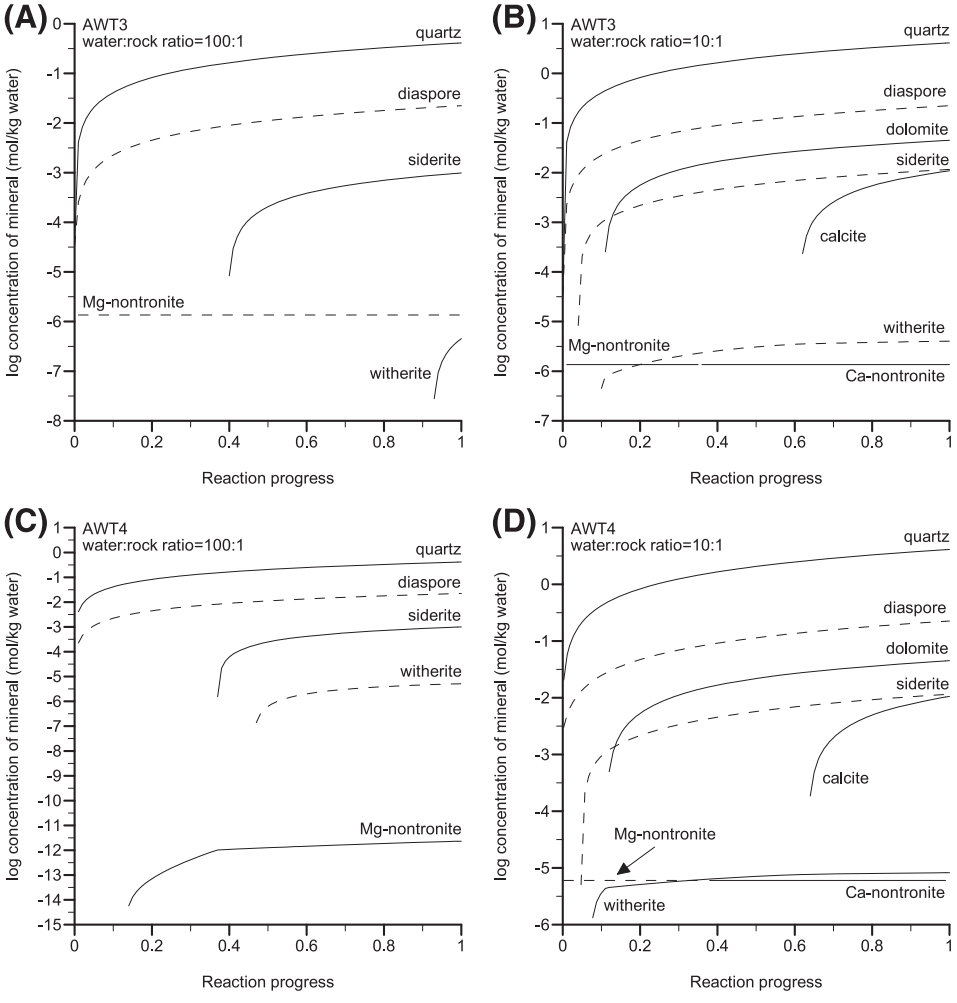

Figure 8. Predicted mineral precipitation for stage 2 of the reaction-path modeling for (A) model fluid AWT3 and a final water–rock ratio of 100:1; (B) model fluid AWT3 and a final water–rock ratio of 10:1; (C) model fluid AWT4 and a final water–rock ratio of 100:1; and (D) model fluid AWT4 and a final water–rock ratio of 10:1. Ca = calcium; Mg = magnesium.

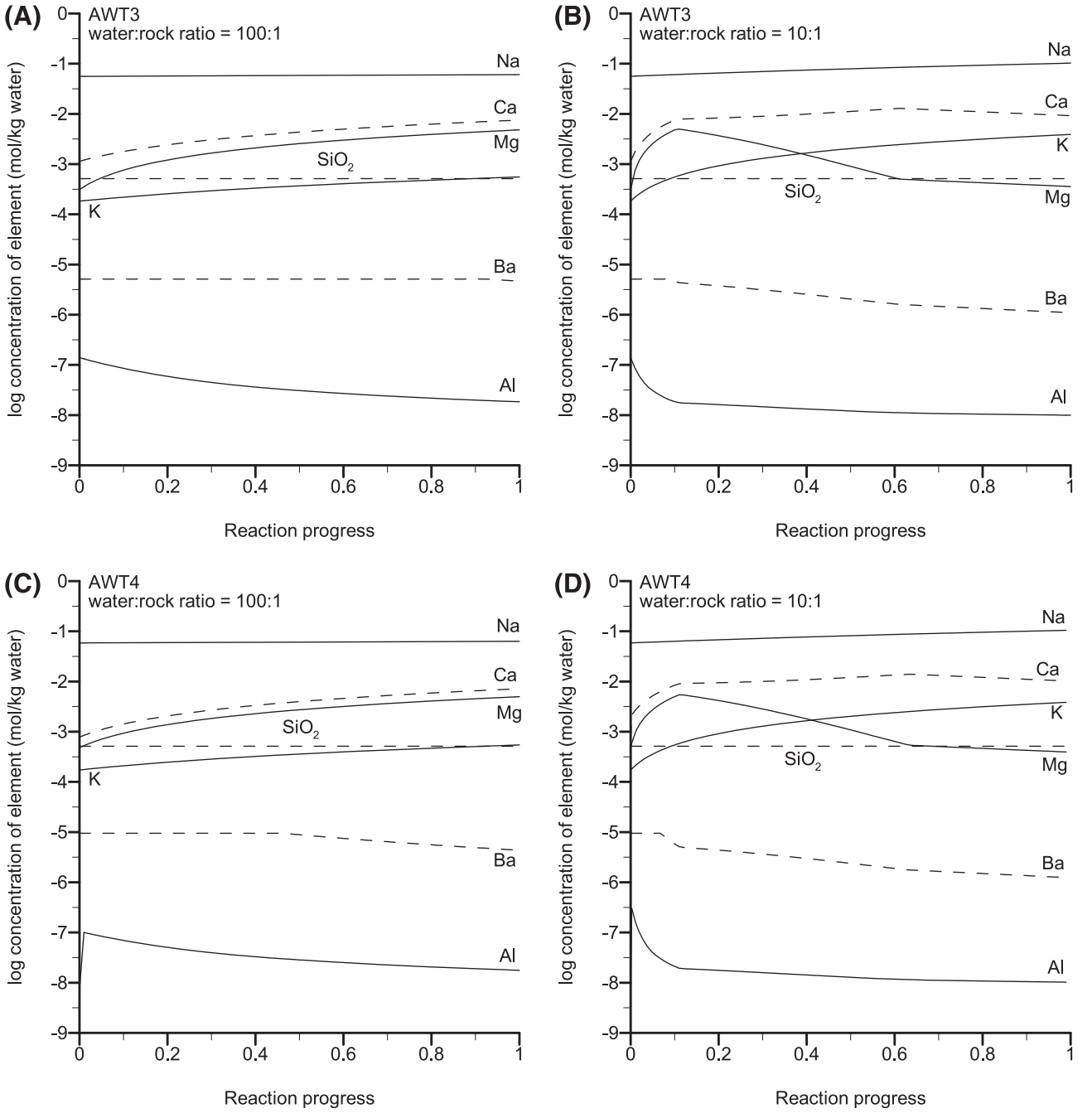

Figure 9. Predicted changes in total elemental concentration during stage 2 of the reaction-path modeling for (A) model fluid AWT3 and a final water–rock ratio of 100:1; (B) model fluid AWT3 and a final water–rock ratio of 10:1; (C) model fluid AWT4 and a final water–rock ratio of 100:1; and (D) model fluid AWT4 and a final water–rock ratio of 10:1. Al = aluminum; Ba = barium; Ca = calcium; K = potassium; Mg = magnesium; Na = sodium; SiO_2 = silicon dioxide.

rock had reacted with the water to raise the pH to approximately 4.5.

Changes in aqueous elemental concentrations as a function of progressive reaction with the Morrow B host rock are shown in Figure 9. During high water–rock ratios, total aqueous concentrations of Na, Mg, potassium (K), and Ca increased because of dissolution of albite, calcite, chlorite, montmorillonite, and illite. Increasing reactions with rock led to eventual decreases in the aqueous concentrations, first of Mg and then of Ca, as dolomite began precipitating and then calcite began reprecipitating. The concentration

of aqueous silicon dioxide remained constant, because quartz remained saturated throughout all of the simulations. The total carbon concentration in both model fluids remained effectively constant for the high water–rock ratio scenario, indicating that carbonate-mineral dissolution was balanced by carbonate-mineral precipitation (Figure 10). With increased rock reaction, carbonate-mineral precipitation exceeded carbonate-mineral dissolution, resulting in an approximately 0.02 mol/kg decrease in total carbon concentration in both model fluids by the end of the low water–rock ratio scenarios (Figure 10). The aqueous concentration of Al in all simulations decreased progressively because of the precipitation of the Al-bearing minerals, diaspore, and nontronite. The aqueous concentration of barium (Ba) held relatively constant during high water–rock ratios, but as the amount of reaction with the host rock increased, the Ba concentration in the model fluids began to decrease with the onset of witherite precipitation.

All of the simulations predicted net dissolution of the host rock. For the 100:1 water–rock simulations, the volume of the host rock decreased by approximately 3.6% for model fluid AWT3 and by approximately 3.5% for model fluid AWT4, which suggests that porosity would have increased by those amounts. For the 10:1 water–rock simulations, porosity increases were smaller, at approximately 0.15% for model fluid AWT3 and approximately 0.14% for model fluid ATW4.

The approximately 75°C temperature of the Morrow B Sandstone lies within a transitional temperature range where the kinetics of quartz precipitation become slow enough such that amorphous silica might be expected to precipitate metastably instead of thermodynamically more stable quartz. In the reaction-path simulations, precipitated silica is in the form of quartz and is mostly reprecipitated quartz from the host rock that was forced to dissolve in the simulation to achieve the desired water–rock ratios, despite the fact that quartz was saturated in the formation water. However, some additional silica was released into solution because of the dissolution of albite, chlorite, montmorillonite, and illite. If this additional silica precipitated as amorphous silica instead of quartz, then, because of the lower density of amorphous silica (2.07 g/cm^3 [1.20 oz/in.^{3}]) compared with quartz (2.65 g/cm^3 [1.53 oz/in.^{3}]), the volume of the host rock would have decreased by only 1.7% instead of 3.5% to 3.6% for a water–rock ratio of 100:1, and the volume of the host rock would have increased by approximately 2% instead of decreasing by approximately 0.14% to 0.15% for a water–rock ratio of 10:1.

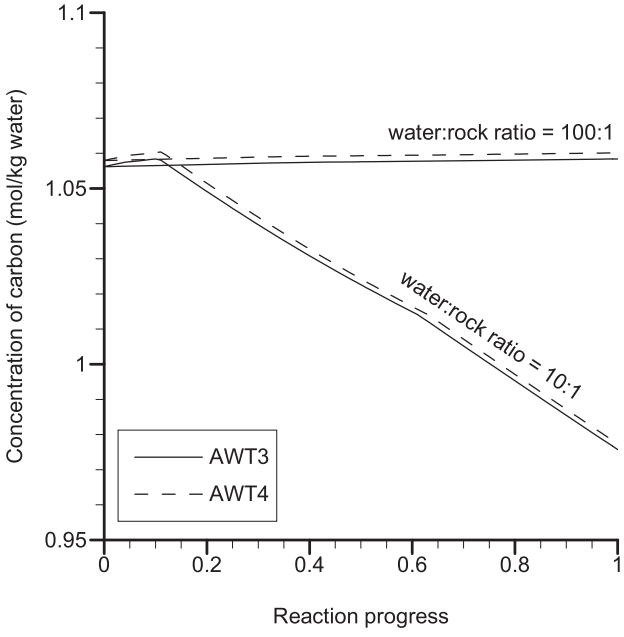

Figure 10. Predicted changes in the concentration of total dissolved carbon for stage 2 of the reaction-path modeling for model fluids AWT3 and AWT4 and final water–rock ratios of 100:1 and 10:1.

DISCUSSION

The results of this study suggest that the Morrow B Sandstone would be an overall geochemically favorable target for CO_2 sequestration. The predominance of quartz in the sandstone and the low salinity of the pore fluid combine to make the system resistant to major mineralogical changes. The Morrow B is predicted to remain composed of predominantly quartz, with the abundance of quartz increasing by approximately 10% from the initial abundance in all simulations. The growth in quartz abundance comes at the expense of silicate accessory minerals, mainly albite, which are converted to diaspore and nontronite. However, diaspore, the second-most abundant mineral formed in the reaction-path simulations, is more than an order of magnitude less abundant than quartz.

Uncertainty in the water–rock ratio of reaction leads to significant uncertainty in the results. However, as CO_2-charged water migrated farther through the Morrow B from the injection well, the water would progressively react with more rock, such that the low water–rock scenario would probably more closely

represent long-term conditions. Thus, the long-term change in porosity, especially farther from the injection well, is likely to be closer to the approximately 0.14% to 0.15% range predicted in the 10:1 water–rock ratio scenario than to the 3.5% to 3.6% range predicted by the 100:1 water–rock ratio scenario. In addition, the pH of the CO_2-charged fluid is more likely to be buffered to a value above 5 instead of below 5, allowing more carbonate-mineral precipitation and a net decrease in dissolved carbon concentration instead of a net increase (Figure 10). However, the low TDS content of the Morrow B formation water and low abundance of minerals in the Morrow B that contain cations readily capable of forming carbonate minerals mean that the total amount of carbonate-mineral precipitation is restricted to approximately 0.3% of the total rock volume for the 100:1 water–rock ratio case and approximately 2.3% to 2.4% of the total rock for the 10:1 water–rock ratio case. Thus, a maximum of only approximately 2% of the 46 g of CO_2 per kilogram of water (0.046 lb CO_2/lb water) at CO_2 saturation is consumed to form carbonate minerals in the model scenarios investigated. This means that the typical assumption regarding the relative factors of solubility versus mineral trapping holds; specifically, much more CO_2 would likely be sequestered by solubility trapping than by mineral trapping (Benson and Cole, 2008). This is particularly true for quartz-rich sandstone aquifers, though the amount of carbonate-mineral precipitation can become greater than predicted for the Morrow B Sandstone in the present study as the salinity of the formation water and the abundance of reactive accessory minerals like Fe phyllosilicates increase (Gunter et al., 2000; Xu et al., 2004; Zerai et al., 2006; Parry et al., 2007; Carroll et al., 2013).

Numerous additional factors not considered in the present study could affect the fate of CO_2 injected into the Morrow B Sandstone, including dissolution into hydrocarbon phases, reaction kinetics, advective transport of CO_2 both as a separate immiscible phase and as a solute in the hydrocarbon and aqueous phases, and dispersion. Most of these factors would reduce the concentration of CO_2 in the Morrow B formation water and the progress of carbonate-mineral formation reactions. The reaction-path models simulated here also force the dissolution of minerals beyond their solubility. Some minerals, like quartz, then simply reprecipitate at the next reaction step, but other minerals remain dissolved, and their constituents precipitate as different minerals at the next reaction step. Thus, the reaction-path models in this study may accurately predict the sequence of mineral precipitation, dissolution, and fluid composition changes caused by CO_2 injection into the Morrow B formation water but perhaps overpredict changes in mineral abundances and porosity.

CONCLUSIONS

Speciation calculations showed the Morrow B pre–CO_2-injection formation water to be supersaturated with respect to an assemblage of zeolite, clay, carbonate, mica, and aluminum hydroxide minerals and quartz. This assemblage is consistent with a burial diagenetic environment and the quartz-rich nature of the Morrow B in which the principal accessory minerals, feldspars and chlorite, are predicted to dissolve and are observed petrograpically to be undergoing alteration (Munson, 1989; Gallagher, 2014). Addition of CO_2 into the Morrow B formation water to the point of saturation given its current pressure, temperature, and salinity lowered the pH to approximately 4.1 to 4.2. Quartz was predicted to precipitate throughout the CO_2 addition, and diaspore and witherite precipitated more variably.

Reaction of the CO_2-charged formation water with the Morrow B host rock caused the pH to recover to a final value of approximately 4.6 to 4.7 for the 100:1 water–rock ratio scenario and to a final value of 5.1 to 5.2 for the 10:1 water–rock ratio scenario. Diaspore and Mg-nontronite were predicted to precipitate throughout the reaction of the CO_2-charged water with the Morrow B host rock. The carbonate minerals, siderite, witherite, dolomite, and calcite, formed respectively as the pH of the fluid rose. The final amount of precipitated quartz was slightly higher than the amount of reactant quartz because of silica released into solution by alteration of minerals like albite to diaspore and Mg-nontronite. The concentrations of Na, Mg, K, and Ca initially increased as albite, calcite, chlorite, montmorillonite, and illite dissolved, but then Ca and Mg concentrations decreased as dolomite and calcite began to precipitate. The maintenance of quartz saturation throughout the reaction paths caused silica concentration to remain constant. However, Al and Ba concentrations decreased because of diaspore, nontronite, and witherite precipitation.

Mineral trapping would only be a sink for CO_2 at relatively low water–rock ratios, consuming approximately 2% of the 46 g/kg CO_2 (0.046 lb CO_2/lb water) at saturation concentration. At high water–rock ratios, carbonate-mineral precipitation is essentially balanced by carbonate-mineral dissolution, and sequestration is

expected to be significant only by means of solubility trapping, with insignificant contribution from mineral trapping. The overall porosity change at the low model water–rock ratio of 10:1 was on the order of approximately 0.14% to 0.15%. Thus, the hydraulic properties of the Morrow B Sandstone should not be greatly altered by chemical reactions associated with CO_2 injection.

REFERENCES CITED

Ampomah, W., R. S. Balch, and R. B. Grigg, 2015, Analysis of upscaling algorithms in heterogeneous reservoirs with different recovery processes: SPE Production Operations Symposium, Oklahoma City, Oklahoma, March 1–5, 2015, SPE-173588-MS, 18 p., doi:10.2118/173588-MS.

Bachu, S., 2002, Sequestration of CO_2 in geological media in response to climate change: Roadmap for site selection using the transform of the geological space into the CO_2-phase space: Energy Conversion and Management, v. 43, p. 87–102, doi:10.1016/S0196-8904(01)00009-7.

Benson, S. M., and D. R. Cole, 2008, CO_2 sequestration in deep sedimentary formations: Elements, v. 4, p. 325–331, doi:10.2113/gselements.4.5.325.

Bergman, P. D., and E. M. Winter, 1995, Disposal of carbon dioxide in aquifers in the U.S.: Energy Conversion and Management, v. 36, p. 523–526, doi:10.1016/0196-8904(95)00058-L.

Bergman, P. D., E. M. Winter, and Z. Y. Chen, 1997, Disposal of power plant CO_2 in depleted oil and gas reservoirs in Texas: Energy Conversion and Management, v. 38, p. S211–S216, doi:10.1016/S0196-8904(96)00271-3.

Carroll, S. A., W. W. McNab, Z. Dai, and S. C. Torres, 2013, Reactivity of Mount Simon Sandstone and the Eau Claire Shale under CO_2 storage conditions: Environmental Science & Technology, v. 47, p. 252–261, doi:10.1021/es301269k.

Creed, J. T., C. A. Brockhoff, and T. D. Martin, 1994, Method 200.8: Determination of trace elements in waters and wastes by inductively coupled plasma-mass spectrometry, revision 5.4: Cincinnati, Ohio, US Environmental Protection Agency, 57 p.

Duan, Z., and R. Sun, 2003, An improved model calculating CO_2 solubility in pure water and aqueous NaCl solutions from 273 to 533 K and from 0 to 2000 bar: Chemical Geology, v. 193, p. 257–271, doi:10.1016/S0009-2541(02)00263-2.

Gallagher, S. R., 2014, Depositional and diagenetic controls on reservoir heterogeneity: Upper Morrow Sandstone, Farnsworth Unit, Ochiltree County, Texas, master's thesis, New Mexico Institute of Mining and Technology, Socorro, New Mexico, 215 p.

Gunter, W. D., E. H. Perkins, and I. Hutcheon, 2000, Aquifer disposal of acid gases: Modelling of water–rock reactions for trapping of acid wastes: Applied Geochemistry, v. 15, p. 1085–1095, doi:10.1016/S0883-2927(99)00111-0.

Gunter, W. D., B. Wiwchar, and E. H. Perkins, 1997, Aquifer disposal of CO_2-rich greenhouse gases: Extension of the time scale of experiment for CO_2-sequestering reactions by geochemical modeling: Mineralogy and Petrology, v. 59, p. 121–140, doi:10.1007/BF01163065.

Harrison, B., and G. Falcone, 2014, Carbon capture and sequestration versus carbon capture utilisation and storage for enhanced oil recovery: Acta Geotechnica, v. 9, p. 29–38, doi:10.1007/s11440-013-0235-6.

Hay, R. L., 1986, Geologic occurrence of zeolites and some associated minerals: Pure and Applied Chemistry, v. 58, p. 1339–1342, doi:10.1351/pac198658101339.

Higley, D. K., 2011, Undiscovered petroleum resources for the Woodford Shale and Thirteen Finger Limestone-Atoka shale assessment units, Anadarko Basin: US Geological Survey Open-File Report 2011–1242, 3 sheets, accessed June 15, 2016, http://pubs.usgs.gov/of/2011/1242/.

Intergovernmental Panel on Climate Change, 2005, IPCC special report on carbon dioxide capture and storage, prepared by Working Group III of the Intergovernmental Panel on Climate Change: Cambridge, United Kingdom, Cambridge University Press, 442 p.

Johnson, K. S., 1989, Geologic evolution of the Anadarko basin, *in* K. S. Johnson, ed., Anadarko Basin Symposium 1988: Norman, Oklahoma, Oklahoma Geological Survey Circular 90, p. 3–12.

Johnson, J. W., E. H. Oelkers, and H. C. Helgeson, 1992, SUPCRT92: A software package for calculating the standard molal thermodynamic properties of minerals, gases, aqueous species, and reactions from 1 to 5000 bar and 0 to 1000°C: Computers & Geosciences, v. 18, p. 899–947, doi:10.1016/0098-3004(92)90029-Q.

McKay, R. H, and J. T. Noah, 1996, Integrated perspective of the depositional environment and reservoir geometry, characterization, and performance of the Upper Morrow Buckhaults Sandstone in the Farnsworth Unit, Ochiltree County, Texas, *in* K. S. Johnson, ed., Deltaic Reservoirs in the Southern Mid-Continent, 1993 Symposium: Norman, Oklahoma, Oklahoma Survey Circular 98, p. 101–114.

Munson, T. W., 1988, Depositional, diagenetic, and production history of the Upper Morrowan Buckhaults Sandstone, Farnsworth Field, Ochiltree County Texas, master's thesis, West Texas University, Canyon, Texas, 117 p.

Munson, T. W., 1989, Depositional, diagenetic, and production history of the Upper Morrowan Buckhaults Sandstone, Farnsworth Field, Ochiltree County Texas: Shale Shaker, v. 40, no. 13, p. 2–20.

Oelkers, E. H., S. R. Gislason, and J. Matter, 2008, Mineral carbonation of CO_2: Elements, v. 4, p. 333–337, doi:10.2113/gselements.4.5.333.

Parker, R. L., 1956, Farnsworth Morrow Oil Field: The Panhandle Geonews, v. 4, no. 1, p. 5–12.

Parry, W. T., C. B. Forster, J. P. Evans, B. B. Bowen, and M. A. Chan, 2007, Geochemistry of CO_2 sequestration in the Jurassic Navajo Sandstone, Colorado Plateau, Utah: Environmental Geosciences, v. 14, no. 2, p. 91–109, doi:10.1306/eg.07120606004.

Puckette, J., Z. Al-Shaieb, and E. Van Evera, 2008, Sequence stratigraphy, lithofacies, and reservoir quality, upper Morrow sandstones, northwestern shelf, Anadarko Basin, *in* R. D. Andrews, ed., Morrow and Springer in the southern midcontinent, 2005 symposium: Norman, Oklahoma, Oklahoma Geological Survey Circular 111, p. 81–97.

Swanson, D. C., 1979, Deltaic deposits in the Pennsylvanian upper Morrow Formation of the Anadarko basin, *in* N. J. Hyne, ed., Pennsylvanian sandstones of the mid-continent: Tulsa, Oklahoma, Tulsa Geological Society Special Publication 1, p. 115–168.

Verma, M. K., 2015, Fundamentals of carbon dioxide-enhanced oil recovery (CO_2-EOR)—A supporting document of the assessment methodology for hydrocarbon recovery using CO_2-EOR associated with carbon sequestration: US Geological Survey Open-File Report 2015–1071, 19 p.

Xu, T., J. A. Apps, and K. Pruess, 2004, Numerical simulation of CO_2 disposal by mineral trapping in deep aquifers: Applied Geochemistry, v. 19, p. 917–936, doi:10.1016/j.apgeochem.2003.11.003.

Zerai, B., B. Z. Saylor, and G. Matisoff, 2006, Computer simulation of CO_2 trapped through mineral precipitation in the Rose Run Sandstone, Ohio: Applied Geochemistry, v. 21, p. 223–240, doi:10.1016/j.apgeochem.2005.11.002.